Journal of Solid State Chemistry 185 (2012) 213–218

Contents lists available at SciVerse ScienceDirect

Journal of Solid State Chemistry

journal homepage: www.elsevier.com/locate/jssc

Structural studies of magnesium nitride fluorides by powder neutron diffraction

Michael A. Brogan [a,1], Robert W. Hughes [b], Ronald I. Smith [c], Duncan H. Gregory [b,*]

[a] School of Chemistry, University of Nottingham, Nottingham NG7 2RD, United Kingdom
[b] WestCHEM, School of Chemistry, University of Glasgow, Glasgow G12 8QQ, United Kingdom
[c] ISIS Pulsed Neutron and Muon Source, Science and Technology Facilities Council, Rutherford Appleton Laboratory, Harwell Oxford, Didcot OX11 0QX, United Kingdom

ARTICLE INFO

Article history:
Received 22 September 2011
Received in revised form
31 October 2011
Accepted 6 November 2011
Available online 15 November 2011

Keywords:
Nitride
Fluoride
Neutron diffraction
Structure
Rock-salt
Paramagnetism

ABSTRACT

Samples of ternary nitride fluorides, Mg_3NF_3 and Mg_2NF have been prepared by solid state reaction of Mg_3N_2 and MgF_2 at 1323–1423 K and investigated by powder X-ray and powder neutron diffraction techniques. Mg_3NF_3 is cubic (space group: $Pm3m$) and has a structure related to rock-salt MgO, but with one cation site vacant. Mg_2NF is tetragonal (space group: $I4_1/amd$) and has an *anti*-$LiFeO_2$ related structure. Both compounds are essentially ionic and form structures in which nitride and fluoride anions are crystallographically ordered. The nitride fluorides show temperature independent paramagnetic behaviour between 5 and 300 K.

1. Introduction

Metal nitride fluorides are a relatively unexplored class of inorganic materials [1,2]. Andersson referred to these as "pseudo-oxides" as they have compositions derived from oxides effectively by the substitution of O^{2-} ions by N^{3-} and F^- ions [3]. The first examples of these were magnesium nitride fluorides prepared by Andersson [4,5] and three phases were reported which had structures related to the rocksalt structure of MgO. Mg_3NF_3 is cubic with N^{3-} and F^- crystallographically ordered and one quarter of the Mg^{2+} sites are empty in an ordered fashion. L-Mg_2NF, a low temperature polymorph, is tetragonal with ordered anions and contains magnesium in square-pyramidal co-ordination. The high temperature polymorph, H-Mg_2NF, is observed after treating L-Mg_2NF at high temperature and pressure (1100–1350 °C; 25–30 kbar). It is cubic and isostructural with MgO with the N^{3-} and F^- anions disordered. Magnesium oxide, MgO, and related compounds have found considerable applications as refractory ceramics [6], catalyst supports [7–9] and recently as additives in the firing of biomass fuels [10].

Following the discovery of the magnesium nitride fluorides, investigations by Ehrlich et al. produced further alkaline earth metal compounds, Ca_2NF, Sr_2NF and Ba_2NF, which were all reported from powder diffraction evidence to be isostructural with the respective group 2 rocksalt-type oxides [11]. Galy et al. also reported Ca_2NF as a rocksalt structure from powder measurements [12]. More recent single crystal X-ray diffraction experiments have, however, identified alternative structures for some of these compounds. Nicklow et al. reported a Ca_2NF phase isostructural with L-Mg_2NF [13]. Under slightly different conditions the same group reported a Ca_2NF phase with a structure in which the simple rock salt cubic cell parameter is doubled due to the anion ordering of N^{3-} and F^- [14]. This doubled, ordered rock salt-type structure is also observed for Sr_2NF [15], but as one progresses further down group 2, single crystal studies reveal that the equivalent barium compound, Ba_2NF, forms with a simple NaCl structure with disordered anions, in agreement with the earlier work of Ehrlich et al. [16]. Recently Ba_2NF was reported to form also with a layered *anti*-α-$NaFeO_2$ structure from powder neutron diffraction measurements [17]. This structure consists of a cubic close packed arrangement of Ba^{2+} cations, with the N^{3-} and F^- anions ordered over the octahedral interstices to produce alternating layers comprising either edge-sharing NBa_6 or FBa_6 octahedra—a structure type more usually observed for alkaline earth metal nitride chlorides, bromides and iodides [18].

Rare earth nitride fluorides were also discovered in the early 1970s. Tanguy et al. initially reported compounds in the solid solution LaN_xF_{3-3x} with a stability range $x=0.34$–0.54 [19]. Cerium forms an analogous solid solution CeN_xF_{3-3x} otherwise

* Corresponding author. Fax: +44 141 330 4888.
E-mail address: Duncan.Gregory@glasgow.ac.uk (D.H. Gregory).
[1] Current address: PANalytical Ltd., 7310 IQ Cambridge, Waterbeach, Cambridge CB25 9AY, United Kingdom.

0022-4596/$ - see front matter © 2011 Elsevier Inc. All rights reserved.
doi:10.1016/j.jssc.2011.11.008

differing from La only in the solubility range ($x=0.33$–0.50) [20]. By contrast, Gadolinium forms only the line phase, Gd_3NF_6 [21] and more recently Pr_3NF_6 and Ce_3NF_6 were prepared and studied by neutron diffraction [22]. The structures of these compounds are related to fluorite, although all show an anion excess and for Ln=Ce and Pr, neutron diffraction has indicated the existence of fluorine interstitials.

Variation in stoichiometry, structure and anion distribution within ternary nitride halide systems is likely to have profound effects on electronic properties, but reports on this are limited. DFT calculations performed by Fang et al. on compounds in the Mg–N–F ternary system show a decreasing band gap from insulating MgF_2 (calculated direct band gap, E_g, of 6.8 eV) through Mg_3NF_3 ($E_g=3.6$ eV) and L-Mg_2NF ($E_g=2.1$ eV) to semiconducting Mg_3N_2 with a calculated direct band gap of 1.6 eV (2.8 eV experimentally) [23].

In this work we report the solid state synthesis of the nitride fluoride Mg_3NF_3 and the low temperature polymorph of the dimagnesium nitride fluoride, L-Mg_2NF and provide detailed models of their crystal structures from powder neutron diffraction experiments. Powder neutron diffraction has allowed us to establish the distribution of nitride and fluoride in these "pseudo-oxides" without ambiguity and to draw conclusions as to the type of bonding in these compounds. We also report the magnetic behaviour of the nitride fluorides.

2. Experimental details

2.1. Starting materials

Magnesium nitride, Mg_3N_2 was prepared by reaction of the pure metal (Alfa 99.9%) with nitrogen using liquid sodium (Riedel-Haën, $>99\%$) as a solvent. All manipulations were carried out in an inert atmosphere. In an argon-filled glovebox a piece of magnesium (ca. 15 g) was cut from a larger ingot and the covering oxide layer physically removed with a file. The clean magnesium metal was submerged in molten sodium contained within a stainless steel crucible. The crucible was then sealed inside a stainless steel reaction vessel fitted with a cold finger. The vessel was heated for 72 h at 1023 K under 1 bar of nitrogen pressure. Upon cooling, the vessel was placed under a vacuum of 10^{-4} Torr and heated for 24 h at 823 K to remove the sodium. Once cooled to room temperature, the vessel was loaded into a glovebox and opened in a nitrogen atmosphere. Mg_3N_2 was obtained as a yellow-green powdered solid. Phase purity was confirmed using powder X-ray diffraction by comparison to ICDD PDF database (card number 35-778; Supplementary Fig. S1).

2.2. Nitride fluoride synthesis

The ternary magnesium nitride fluorides were prepared by the high temperature solid state reaction of stoichiometric amounts of synthesised Mg_3N_2 with anhydrous MgF_2 (Aldrich, 99.9%). All manipulations were carried out under inert nitrogen or argon atmospheres. The appropriate 1:3 and 1:1 stoichiometric molar ratios were used in the synthesis of Mg_3NF_3 (**1**) and Mg_2NF (**2**) respectively, as shown below:

$$Mg_3N_2+3MgF_2\rightarrow 2Mg_3NF_3 \quad (1)$$

$$Mg_3N_2+MgF_2\rightarrow 2Mg_2NF \quad (2)$$

In an N_2-filled recirculating glovebox, mixtures of the starting materials were thoroughly mixed and ground together using an agate pestle and mortar, after which the samples were pressed into pellets using a hand press inside the glove box. The pellets were then transferred to an evacuable glovebox with a purified argon atmosphere and wrapped in molybdenum foil liners, which serve to prevent unwanted side reactions between the pellet and the stainless steel crucible. The foil-wrapped pellets were sealed inside the stainless steel crucibles using an arc welder within an argon-filled glove box. The sealed crucibles were transferred to a high temperature tube furnace and heated for 5 days at 1323–1423 K under flowing argon to prevent aerial oxidation. The reaction vessels were slowly cooled at 20 K h^{-1} to room temperature following heating and opened in a nitrogen filled glovebox using pipe cutters.

2.3. Characterisation by powder X-ray diffraction (PXD)

All products were initially characterised by PXD. Data were collected using a Philips X-pert diffractometer operating with Cu$K\alpha$ radiation. Initial scans were carried out from $5\leq 2\theta/^\circ\leq 80$ with a step size of 0.02° and a scan time of 50 min. Due to the air-sensitive nature of the products, a dedicated air-tight aluminium sample holder with Mylar windows was employed [24].

Data were analysed by Philips Automated Powder Diffraction software. Phase identification was carried out using the Philips software routine, PC-IDENTIFY to access the ICDD PDF database. Unit cells were indexed using DICVOL91 [25]. Further data were collected over a longer period, from $5\leq 2\theta/^\circ\leq 120$ with a step size of 0.02° over 14 h, in order to obtain data suitable for structure refinement.

2.4. Characterisation by powder neutron diffraction (PND)

Time of flight (ToF) PND data were collected using the medium resolution, high intensity POLARIS diffractometer at the ISIS facility, Rutherford Appleton Laboratory. For each sample, ca. 2 g of material was sealed in a vanadium can, made airtight using an indium wire gasket. All data were collected at 298 K with collection times of 1–2 h. Diffraction data collected using the low angle ($\langle 2\theta\rangle=35^\circ$; d-spacing range $\sim$0.5–8.1 Å), backscattering ($\langle 2\theta\rangle=145^\circ$; d-spacing range $\sim$0.5–3.2 Å) and $\langle 2\theta\rangle=90^\circ$ detector bank (d-spacing range $\sim$0.5–4.2 Å) were used for structure refinement.

2.5. Structure refinement

Rietveld refinement using both the PXD and ToF PND data was performed using the General Structure Analysis System (GSAS) through the windows based EXPGUI interface [26,27]. The overall refinement strategy was largely identical when using either PXD or PND data and employed selected background and peak shape functions as appropriate for the different instruments.

For the PXD refinements, the initial starting models used for **1** and **2** were those proposed by Andersson for Mg_3NF_3 and L-Mg_2NF, respectively [3]. The background coefficients (GSAS Function 7—a linear interpolation function), zeropoint and scale factor were varied initially, followed by refinement of the unit cell parameters. Modelling of the peak shapes was carried out using Function 2, a Simpson's rule integration of the pseudo-Voigt function. The atomic parameters, peak profile parameters and isotropic thermal vibration parameters were subsequently refined. Impurity phases were added once refinement of the main phase was almost complete. The anisotropic thermal vibration parameters of the main phase were one of the last variables to be refined, whilst in the final refinement cycles all parameters were simultaneously varied until convergence was achieved.

For the POLARIS PND refinements, the appropriate starting models derived from the PXD experiments above were refined

against data from the three detector banks. Initially data from the backscattering bank were used for each refinement, with the low angle and 90° histograms added later in the refinement. Initially background coefficients (GSAS Function 6—a combination of power series to account for background contributions at low and high Q) and the scale factor were refined. Unit cell parameters and peak shape were varied subsequently. (Modelling of the peak shapes was carried out using ToF peak shape function 3, a convolution of back-to-back exponentials with a pseudo-Voigt function.) Absorption coefficients, atomic positions, and isotropic thermal vibration parameters were refined once stability and convergence was achieved. Impurity phases were added once refinement of the main phase was almost complete in each case. The anisotropic thermal vibration parameters of the main phase were refined once all other parameters were stable, whilst in the final refinement cycles all parameters were simultaneously varied.

2.6. Magnetic measurements

Variable temperature magnetic susceptibility measurements were performed for both **1** and **2** (ca. 10–25 mg for each sample) using a Quantum Design MPMS-XL 5 T SQUID magnetometer. All samples were loaded in a nitrogen-filled, recirculating glovebox. Data were collected between 5 and 300 K under fields of 1000 Oe with points at 1 K intervals from 5 to 30 K and 5 K intervals between 30 and 300 K. Data were corrected for core diamagnetism and the diamagnetic contribution of the sample holders (gelatine capsules).

3. Results and discussion

3.1. Mg_3NF_3 (**1**)

An off-white powder, Mg_3NF_3 (**1**) was successfully synthesised at 1323 K. Initial powder diffraction measurements produced a pattern that matched the ICDD database entry (PDF Card number 25-0517). Indexing of the peaks gave a cubic unit cell with $a=4.2153(4)$ Å, which is in good agreement with the literature value of 4.216 Å [3]. Longer PXD scans revealed the presence of a small impurity of the MgF_2 reagent, which was included as a secondary phase in the final cycles of the refinement and refined to a final phase fraction of 1.1(2) wt%. Given the similarity in form factor for isoelectronic N^{3-} and F^-, obtaining a definitive structure for **1** in which partial site disorder could be categorically discarded from PXD data alone was not possible. PND data were collected to address this problem as there is sufficient contrast in the coherent neutron scattering lengths to allow a convincing solution to be obtained (N: $b=9.36$ fm, F: $b=5.65$ fm) [28]. Starting from the refined PXD model, the refinement progressed smoothly and converged to produce a good fit to the data. Attempts to refine occupancies of the anion sites to investigate possible N/F disorder reduced the quality of the fit, increased R-factors and caused some parameters to become unstable, indicating an ordered model in which N^{3-} occupies only the 1*b* (1/2, 1/2, 1/2) site and F^- the 3*d* (1/2, 0, 0) site to be correct. The details of the both PXD and PND refinements can be found in Table 1. Important interatomic distances can be found in Table 2. A fitted profile plot for the PND data for the backscattering bank ($\langle 2\theta \rangle = 145°$) is shown in Fig. 1. (Additional refinement fits and a table of anisotropic thermal displacement parameters can be found in the Supplementary information.)

The structure of **1** (Fig. 2) is related to that of MgO, with N^{3-} and F^- replacing O^{2-} in an ordered fashion in the cubic unit cell. Perhaps the key difference between **1** and MgO lies with the

Table 1
Refined crystallographic parameters for (**1**) from PXD and PND at 298 K.

Compound		Mg_3NF_3	Mg_3NF_3
Radiation		X-ray	Neutron
Instrument		Philips X'pert	POLARIS
Space group		*Pm*3*m*	
Crystal system		Cubic	
Formula weight		143.917	
Z		1	
***a* (Å)**		4.2126 (1)	4.21404 (2)
Cell volume, V (Å^3)		74.754 (4)	74.834 (1)
$U_{iso}/U_{eq} \times 100$ (Å^2)	**Mg** (3*c*) (0,1/2,1/2)	4.05 (5)	5.46 (3)
	N (1*b*) (1/2,1/2,1/2)	3.95 (5)	7.94 (3)
	F (3*d*) (1/2, 0, 0)	4.48 (5)	3.54 (4)
No. of data points		3577	15109
R_{wp}		0.1186	0.0328
R_p		0.0771	0.0469
χ^2		6.39	4.101

Table 2
Important interatomic distances and angles for **1**.

	PXD	PND
Mg–Mg (Å)	2.9787 (1)	2.9798 (1)
Mg–F (Å)	2.1065 (1)	2.1070 (1)
Mg–N (Å)	2.1063 (1)	2.1070 (1)
Mg–N–Mg (deg.)	90/180	90/180
Mg–F–Mg (deg.)	90/180	90/180

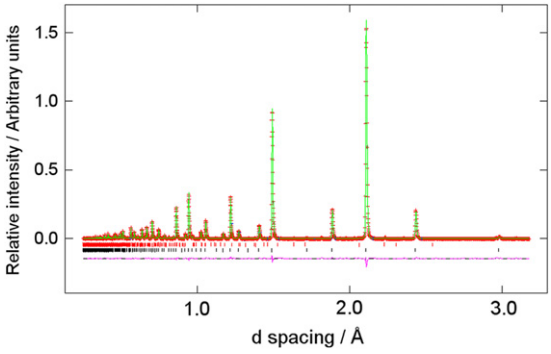

Fig. 1. Observed, calculated and difference profile plot for Mg_3NF_3 (**1**) from neutron refinement ($\langle 2\theta \rangle = 145°$ bank). Crosses are observed data; the solid line is the calculated profile. The difference profile is shown below. Vertical bars below the profile mark the reflection positions for Mg_3NF_3 (lower) and MgF_2 (upper).

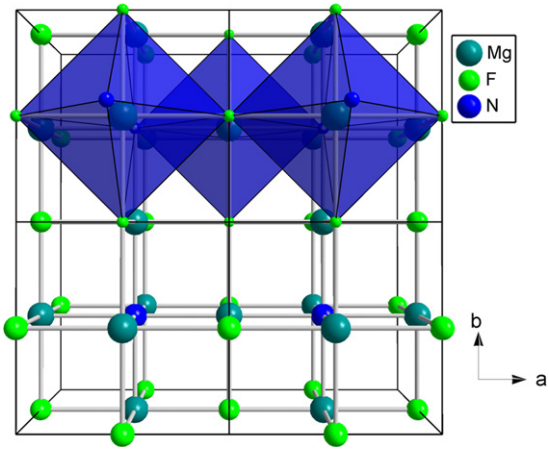

Fig. 2. Structural representation of Mg_3NF_3 viewed down the *c*-axis. $Mg(N,F)_6$ octahedra are highlighted.

cation–anion ratio and hence defect structure. In MgO there is a 1:1 ratio of cations to anions with Mg located on the 4*a* site in the ideal rock salt structure (space group $Fm-3m$) whereas in Mg_3NF_3 there is a 3:4 ratio of cations to anions. In the resulting primitive cell of the nitride fluoride (space group $Pm-3m$), Mg is situated on the 3*c* (0, 1/2, 1/2) site with the (0, 0, 0) site of the rock salt structure vacant. Magnesium is octahedrally co-ordinated to two nitride anions and four fluoride anions. The Mg–N (Mg–F) bond distance is 2.1070 (1) Å, which is in excellent agreement with the literature value of 2.108 (1) Å [3]. This is also very close to the Mg–O bond length of 2.1061 (1) Å in the rock salt structure of the oxide [29]. The distance also falls within the range of Mg–N bonds seen in the *anti*-bixbyite Mg_3N_2 (2.084 (1)–2.179 (1) Å) [30] although is slightly longer than the Mg–F bond length in the binary fluoride (1.984 (2)–1.994 (1) Å) [31]. The Mg–Mg distance is 2.980 (1) Å which is longer than in Mg_3N_2 (2.716 (1) Å) but shorter than that found in MgF_2 (3.045 (3) Å) and Mg metal itself (3.1903 (1)–3.2025 (1) Å) [32].

Bond valence calculations using the PND structure as a basis were performed using the VALENCE software [33]. Applying the parameters of Brese and O'Keeffe (R_{ij}(Mg–N)=1.85, R_{ij}(Mg–F)=1.58, b=0.37) [34] gives sums of 1.96 for Mg, 3.00 for N and 0.97 for F. The results would thus imply that the bonding in M_3NF_3 is very close to purely ionic and that the Mg–N bond in the nitride fluoride is among the most ionic metal–nitrogen bonds in the solid state. Similarly the Mg…Mg interaction cannot be viewed as so significant in Mg_3NF_3 as it appears to be in Mg_3N_2 [24]. Certainly DFT calculations would also suggest that with F 2*p*, N 2*p* and unoccupied 3*s* states well separated the nitride fluoride can be viewed as ionic [17].

3.2. Mg_2NF (**2**)

The synthesis of a pale cream powder of **2** was achieved at 1423 K. Initial experiments had shown that a higher temperature was required for formation of **2** otherwise a small impurity of **1** was always observed. Powder diffraction measurements showed a match to the pattern for the previously reported low temperature phase of Mg_2NF (ICDD Card number 25-0516). The reflections could be indexed to a tetragonal unit cell with a=4.1816(4) Å and c=10.0322(6) Å which compares well with the literature values of a=4.186 Å and c=10.042 Å [3]. As for **1**, initial Rietveld refinement of **2** was performed against PXD data. The refinement progressed smoothly and gave a good fit to the data using the L-Mg_2NF structure as a starting model.

PND data were collected for **2** and a refinement taking the PXD model as the starting point progressed smoothly and converged to produce a good fit to the data. As with **1**, possible disorder was investigated by attempting to vary the anion occupancies but doing so always resulted in increases to the residuals and/or physically unrealistic parameters. Parameters from both the PXD and PND refinements of **2** can be found in Table 3. Important interatomic distances are displayed in Table 4. The profile plot for the refinement against PND data for the backscattering bank ($\langle 2\theta \rangle = 145^\circ$) is shown in Fig. 3. (Further PXD and PND refinement results and a table of anisotropic thermal displacement parameters can be found in the Supplementary information.)

The structure adopted by **2** is *anti*-$LiFeO_2$ type (Fig. 4), where F^- occupies the equivalent Fe^{3+} position, N^{3-} occupies the equivalent Li^+ position and Mg^{2+} is located on the equivalent anion (O^{2-}) site. The structure can be viewed as an intermediate structure between that of rock salt and zinc blende. The magnesium cation in **2** is co-ordinated to three nitride and two fluoride anions in a square pyramidal co-ordination. An additional, longer Mg–F interaction completes a distorted, axially extended octahedron (Fig. 5). The Mg–N/F bond distances in the pyramid base are 2.1253 (1) Å with the apical Mg–N bond at 2.1393 (1) Å. As for **1** these fall within typical Mg–N bond length ranges seen in Mg_3N_2 (2.084 (1)–2.179 (1) Å), and are slightly longer than Mg–F bonds in MgF_2 (1.984 (2)–1.994 (1) Å) [24,25]. The additional Mg–F distance lies at 2.8730 (1) Å. The Mg–Mg distance is 2.7430 (1) Å, which is closer to that in Mg_3N_2 (2.716 (1) Å) than in MgF_2 (3.045 (3) Å) or Mg metal (3.1903 (1)–3.2025 (1) Å).

Bond valence calculations performed using the structure refined from PND data and the same r_{ij} and b parameters used

Table 3
Refined crystallographic parameters for (**2**) from PXD and PND at 298 K.

Compound		Mg_2NF	Mg_2NF
Radiation		X-ray	Neutron
Instrument		X'pert	POLARIS
Space group		$I4_1/amd$[a]	
Crystal system		Tetragonal	
Formula weight		81.615	
Z		4	
***a* (Å)**		4.1847 (1)	4.18687 (2)
***c* (Å)**		10.0223 (1)	10.0247 (1)
Cell volume, *V* (Å^3)		175.51 (1)	175.73 (2)
$U_{iso}/U_{eq} \times 100$ (Å^2)	**Mg** (*8e*) (0,0,*z*)	2.13 (2)	0.66 (1)
	N (*4b*) (0,0, 1/2)	2.04 (1)	0.52 (1)
	F (*4a*) (0,0,0)	1.77 (2)	1.59 (1)
Mg (0, 0, *z*)[b]	***z***	0.2868 (1)	0.2866 (1)
No. of data points		5692	15,267
R_{wp}		0.1668	0.0273
R_p		0.1242	0.0492
χ^2		2.263	3.865

[a] Origin choice 1.
[b] For comparison, the *z* value from Ref. [3] converted to Origin choice 1 would be 0.2845.

Table 4
Important interatomic distances and angles for **2**.

	PXD	PND
Mg–Mg (Å)	2.7365 (1)	2.7430 (1)
1 × Mg–F (Å)	2.8757 (1)	2.8730 (2)
2 × Mg–F (Å)	2.1240 (1)	2.1253 (1)
1 × Mg–N (Å)	2.1336 (1)	2.1393 (1)
2 × Mg–N (Å)	2.1240 (1)	2.1253 (1)
4 × F/N_{eq}–Mg–N_{ax} (deg.)	100.06 (1)	99.94 (1)
4 × F/N_{eq}–Mg–F/N_{eq} (deg.)	88.25 (1)	88.29 (1)
2 × F/N_{eq}–Mg–F/N_{eq} (deg.)	159.89 (1)	160.12 (1)
4 × F/N_{eq}–Mg–F_{ax} (deg.)	79.94 (1)	80.06 (1)
1 × N_{ax}–Mg–F_{ax} (deg.)	180.00	180.00

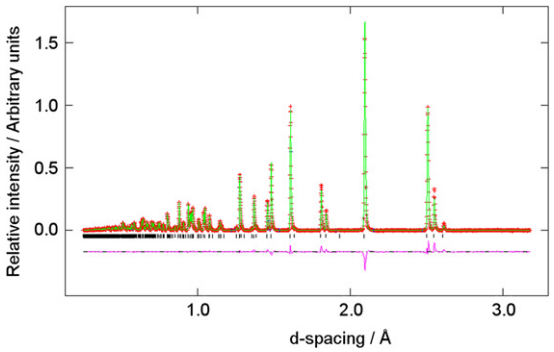

Fig. 3. Observed, calculated and difference profile plot for Mg_2NF (**2**) from neutron refinement ($\langle 2\theta \rangle = 145^\circ$ bank). Crosses are observed data; the solid line is the calculated profile. The difference profile is shown below. Vertical bars below the profile mark the reflection positions for Mg_2NF.

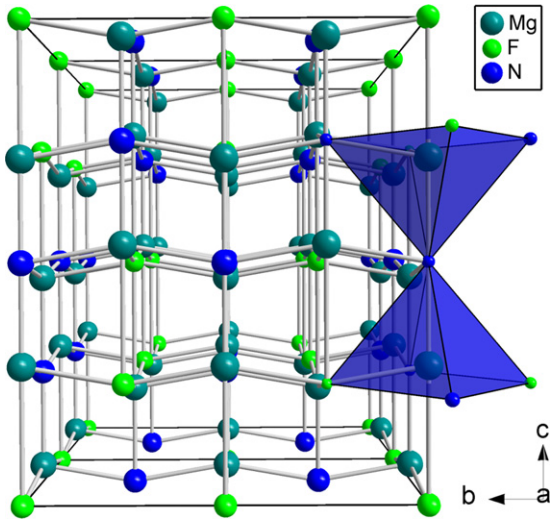

Fig. 4. Structural representation of Mg_2NF viewed down the *a*-axis. $Mg(N,F)_5$ square-based pyramids are highlighted.

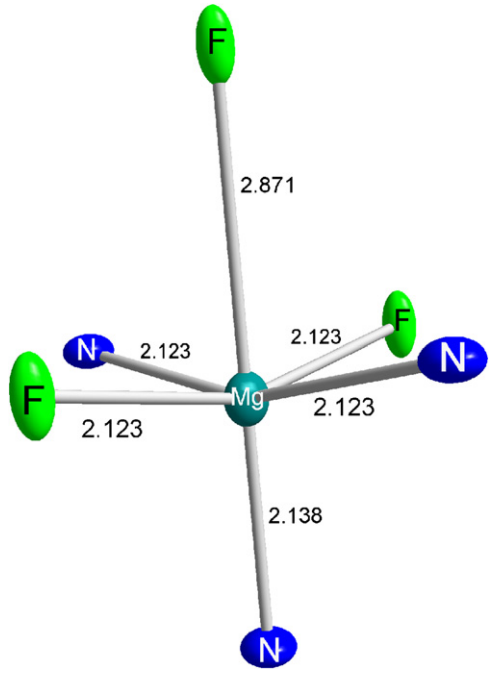

Fig. 5. Local co-ordination around magnesium in Mg_2NF (bond distances in Å). Ellipsoids are shown at 50% probability.

for Mg_3NF_3 above [28], gave sums of 1.90 for Mg, 2.85 for N and 0.92 for F. These values are slightly lower than expected and lower than those found in Mg_3NF_3, above, but nevertheless suggest a strong ionic component to bonding in Mg_2NF. "Underbonding" is not uncommon in nitridic compounds and given, for example, the low values reported for Mg and N in Mg_3N_2, it is likely that Mg…Mg nonbonding interactions could play a role in Mg_2NF as they do in the binary magnesium nitride [24]. It is not totally surprising, therefore, that the members of the Mg–N–F system become more ionic as one increases the fluoride content from Mg_3N_2 through the nitride fluorides Mg_2NF and Mg_3NF_3 to MgF_2.

Bond valence figures can also demonstrate how weak the additional axial Mg–F interaction is. In MgF_2 the bond valence of a single Mg–F bond is 0.336. In **1** the bond valence of Mg–F is 0.241. The square pyramid Mg–F bond in **2** gives a bond valence of 0.230 but the long range Mg–F bond of **2** has a bond valence of only 0.03. Therefore it is tempting to dismiss this connection as a relatively weak interaction rather than classify it as an Mg–F bond.

Analysis of the anisotropic thermal displacement parameters shows that the ellipsoid for the fluorine position is elongated in the *c*-axis, suggestive of some measure of (local) anion disorder or possibly indicative of fluoride ion mobility. This feature is also seen in the isostructural Ca_2NF [11], where the authors carried out refinements with partial oxygen substitution on the F site in an attempt to alleviate the large displacement parameters. In the case of Ca_2NF this model was rejected as it worsened the fit. Attempts to include partial oxygen substitution in our model for **2** also decreased fit quality, and when freely refined, fluorine occupancy always refined back to unity.

3.3. Magnetic measurements

SQUID magnetometry measurements revealed that both samples **1** and **2** exhibit weak temperature independent paramagnetic behaviour (typically $\chi_M \sim 5 \times 10^{-4}$ emu mol^{-1}) between 5 and 300 K. This behaviour is commensurate with other alkaline earth nitride halides and suggests either weakly paramagnetic materials or intrinsically diamagnetic materials with very small levels of alkaline earth metal impurities (below the detection limit of PXD and PND) [15,16]. (A plot of χ_M vs. T for **1** and **2** is available as Supplementary information.)

4. Summary

Two ternary nitride fluorides of magnesium, Mg_3NF_3 and Mg_2NF, have been synthesised via the solid state reaction of appropriate ratios of Mg_3N_2 and MgF_2. Powder neutron diffraction studies have confirmed structures in which the fluoride and nitride anions are completely ordered in both cases. Bond valence calculations reveal that both these nitride fluorides contain among the most ionic metal—nitrogen bonds in the solid state. It is worthy of note that the original work of Andersson provided extremely accurate models for both structures given the stage of development of powder refinement methods at the time of publication [3]. Magnetic measurements demonstrate that both nitride fluorides exhibit very weak paramagnetism with susceptibilities essentially independent of temperature.

Acknowledgments

Neutron beamtime at ISIS was provided by the UK Science and Technology Facilities Council (STFC). DHG thanks the University of Nottingham for funding a studentship for M.A.B., and WestCHEM for funding R.W.H. as a WestCHEM Fellow.

Appendix A. Supplementary Information

Supplementary data associated with this article can be found in the online version at doi:10.1016/j.jssc.2011.11.008.

References

[1] D.H. Gregory, Coord. Chem. Rev. 215 (2001) 301.
[2] D.A. Headspith, M.G. Francesconi, Top. Catal. 52 (2009) 1611.
[3] S. Andersson, Ark. Kemi. 26 (1967) 521.
[4] S. Andersson, Acta Crystallogr. B25 (1969) 1009.
[5] S. Andersson, J. Solid State Chem. 1 (1970) 306.

[6] W.E. Lee, R.E. Moore, J. Am. Ceram. Soc. 81 (1998) 1385.
[7] M.A. Bañares, Catal. Today 51 (1999) 319.
[8] T.V. Choudhary, S. Banerjee, V.R. Choudhary, Appl. Catal. A 234 (2002) 1.
[9] S. Albonetti, F. Cavani, F. Trifirò, Catal. Rev. 38 (1996) 413.
[10] T.R. Miles, T.R. Miles Jr, L.L. Baxter, R.W. Bryers, B.M. Jenkins, L.L. Oden, Biomass Bioenergy 10 (1996) 125.
[11] P. Ehrlich, W. Linz, H. Seifert, Naturwissenschaften 58 (1971) 219.
[12] J. Galy, M. Jaccou, S. Andersson, C.R. Acad. Sci. 272 (1971) 1657.
[13] R.A. Nicklow, T.R. Wagner, C.C. Raymond, J. Solid State Chem. 160 (2001) 134.
[14] D.R. Jack, M. Zeller, T.R. Wagner, Acta Crystallogr. C61 (2005) i6–8.
[15] T.R. Wagner, J. Solid State Chem. 169 (2002) 13.
[16] H. Seibel, T. Wagner, J. Solid State Chem. 177 (2004) 2772.
[17] A.S. Bailey, R.W. Hughes, P. Hubberstey, C. Ritter, R.I. Smith, D.H. Gregory, Inorg. Chem. 50 (19) (2011) 9545.
[18] See for example: A. Bowman, P.V. Mason, D.H. Gregory, Chem. Commun. (2001) 1650;
A. Bowman, R.I. Smith, D.H. Gregory, J. Solid State Chem. 179 (2006) 130;
A. Bowman, R.I. Smith, D.H. Gregory, J. Solid State Chem. 178 (2005) 1807;
M.A. Brogan, R.W. Hughes, R.I. Smith, D.H. Gregory, Dalton Trans. 39 (2010) 7153.
[19] B. Tanguy, M. Pezat, J. Portier, P. Hagenmuller, Mater. Res. Bull. 6 (1971) 57.
[20] M. Pezat, B. Tanguy, M. Vlasse, J. Portier, P. Hagenmuller, J. Solid State Chem. 18 (1976) 381.
[21] B. Tanguy, P. Hagenmuller, J. Portier, M. Pezat, C. R. C274 (1972) 1344.
[22] T. Vogt, E. Schweda, J.P. Laval, B. Frit, J. Solid State Chem. 331 (1989) 324.
[23] C.M. Fang, K.V. Ramanujachary, H.T. Hintzen, G. de With, J. Alloy Compd. 351 (2003) 72.
[24] M.G. Barker, M.J. Begley, P.P. Edwards, D.H. Gregory, S.E. Smith, J. Chem. Soc. Dalton Trans. (1996) 1.
[25] A. Boultif, D.J. Louer, J. Appl. Crystallogr. 24 (1991) 987.
[26] A.C. Larson, R.B. von Dreele, The General Structure Analysis System, Los Alamos National Laboratories, Los Alamos, NM, 2000.
[27] B.H. Toby, J. Appl. Crystallogr. 34 (2001) 210.
[28] V.F. Sears, Neutron News 3 (3) (1992) 26.
[29] N.G. Schmahl, G.F. Eikerling, J. Appl. Crystallogr. 1 (1968) 246.
[30] D.E. Partin, D.J. Williams, M. O'Keeffe, J. Solid State Chem. 132 (1997) 56.
[31] G. Vidal-Valat, J.-P. Vidal, C.M.E. Zeyen, K. Kurki-Suonio, Acta Crystallogr. B35 (1979) 1584.
[32] G.V. Raynor, Proc. R. Soc. London Ser. A 174 (1940) 457.
[33] I.D. Brown, J. Appl. Crystallogr. 29 (1996) 479.
[34] N.E. Brese, M. O'Keeffe, Acta. Crystallogr. B47 (1991) 192.